PCCP

PAPER

View Article Online
View Journal | View Issue

Cite this: *Phys. Chem. Chem. Phys.*, 2015, **17**, 13421

Perspectives on the energy landscape of Au–Cl binary systems from the structural phase diagram of Au_xCl_y ($x + y = 20$)†

Zhimei Tian[ab] and Longjiu Cheng*[a]

Received 31st March 2015,
Accepted 20th April 2015

DOI: 10.1039/c5cp01863c

www.rsc.org/pccp

Ligand-protected gold (Au-L) nanoclusters have attracted much attention, where the reported electronic and geometric structures show great diversity. To give a direct and overall view of the energy landscape of Au-L binary systems, the Au_xCl_y ($x + y = 20$) system is taken as a test case. By intensive global search of the potential energy surface at the level of density functional theory, a diverse set of global minima and low-lying isomers are found at each composition, and the structural phase diagram is obtained. The unbiased global search is carried out using the method combining the genetic algorithm with the TPSS functional. At $x = 10$ with the stoichiometric ratio of Au and Cl (1 : 1), the cluster presents a catenane structure. When x is in the range of 11–20, the clusters are Au-rich, and the Au–Cl system can be viewed as Cl-protected gold nanoclusters, where the gold cores consist of superatoms, superatom networks, or superatomic molecules in electronic structures. At $x = 11$–15, the gold cores consist of Au_3, Au_4 and Au_5 2e-superatoms protected by staple motifs. At $x = 16$–20, the clusters are pyramidal superatomic molecules with one Au_{16} superatom core bonding with the four vertical atoms (Au or Cl). When x is in the scope of 9–5, the clusters are Cl-rich, and the 5d electrons of Au participate in bonding, resulting in high multiplicities. The Au–Cl binary system shows great diversity and flexibility in electronic and geometric structures, and there are corresponding structures to most of the experimentally produced Au-L nanoclusters in our structural phase diagram. We believe that the structural phase diagram gives an overall perspective on the universe of Au-L nanoclusters.

I. Introduction

Gold nanoparticles of 2–3 nm bridge the "material gap", which display a distinct electronic transition in optical absorption, intrinsic magnetism, enhanced photoluminescence, and discontinuous charge transport and redox properties.[1–4] Due to the strong relativistic effects, gold atoms and clusters display many unique properties in chemical bonding. The interaction between gold and thiolate (SR), phosphine (PR_2), and halogen (Cl) is of considerable importance in wide areas of modern science from both fundamental and practical viewpoints.[5,6] The ligand-protected gold Au–SR nanoclusters are of considerable importance for understanding the structural evolution of clusters from small-to-medium sizes and the relative stability of different optimized cluster geometries. Bare gold clusters in the size range $n = 2$–24 have been well-studied, which undergo a series of structural transitions from a planar, flat shell to a cage, pyramid and to a tubular motif.[7–14] For medium-sized gold clusters, the compact core–shell structures are likely a prevalent structural form.[15–19] Ever since 2003, the Au_{20} cluster, which was first revealed by photoelectron spectroscopy, has received much attention.[20–22] The determination of the atomic structure at the nanoscale is a challenge. Experimentally, significant progress has been made in the chemical synthesis of ultrasmall ligand-protected Au nanoclusters. The first major breakthrough in total structure determination was achieved in 2007 by the Kornberg group, who determined the crystal structure of $Au_{102}(SR)_{44}$.[23] Later, several clusters such as $[Au_{25}(SR)_{18}]^-$,[24] $Au_{38}(SR)_{24}$,[25] $Au_{24}(SR)_{20}$,[26] $[Au_{20}(PR_2)_{10}Cl_4]Cl_2$,[27] and $Au_{36}(SR)_{24}$ (ref. 28) were experimentally determined. Structures of the experimentally synthesized ligand-protected gold (Au-L) nanoclusters can be well predicted by density functional theory (DFT) calculations and the success of DFT method in understanding and predicting the structures of Au–SR clusters is truly inspiring.[29–31]

The reported Au-L nanoclusters present various forms of electronic structures, including superatoms, superatom networks,

[a] *Department of Chemistry, Anhui University, Hefei, Anhui, 230601, China. E-mail: clj@ustc.edu*
[b] *School of Chemistry and Materials Engineering, Fuyang Teachers College, Fuyang, Anhui, 236037, China*

† Electronic supplementary information (ESI) available: The symmetries and relative energies of the low-lying isomers are given in Fig. S1 and S2, respectively. The superatomic models and AdNDP localized natural bonding orbitals of 17I, 18I and 19I clusters are collected in Fig. S3–S5. See DOI: 10.1039/c5cp01863c

superatomic molecules, *etc.* To understand the intrinsic stability of Au–SR nanoclusters, Häkkinen and co-workers proposed the superatom complex concept based on the jellium model.[32] According to the concept, one determines the valence-electron count (V) of the $Au_m(SR)_n^q$ cluster (where q is the charge of the cluster) using $V = m - n - q$. Each gold atom contributes one valence electron and each SR localizes one electron; if there are halogen groups in the cluster, each halogen also localizes one electron.[33] The appropriate Aufbau rule of super shells for spherical Au clusters is $|1S^2|1P^6|1D^{10}|2S^21F^{14}|2P^61G^{18}|\ldots$ (S–P–D–F–G–H– denote angular-momentum characters), associated with magic numbers 2, 8, 18, 34, 58,...[32] Superatom theory has achieved great success in prediction of the stability of thiolate-protected gold nanoparticles, which can be understood by the magic numbers. Jiang *et al.* recently proposed $[Au_{12}(SR)_9]^+$, $Au_8(SR)_6$, $Au_{10}(SR)_8$ and $Au_{15}(SR)_{13}$ clusters for the magic number 2.[34,35] $[Au_{25}(SR)_{18}]^-$ is associated with the magic number 8.[24] $[Au_{44}(SR)_{28}]^{2-}$ corresponds to the magic number 18.[36] $Au_{102}(SR)_{44}$ is associated with the magic number 58.[37,38]

The superatom model can treat only those clusters with a spherical core, however, the stability of clusters with non-spherical cores cannot be understood. In addition, not all the Au–SR clusters exhibit magic numbers of free valence electrons as described by the spherical jellium model. According to the superatom model, $Au_{38}(SR)_{24}$ has 14 valence electrons, and $Au_{18}(SR)_{14}$, $Au_{20}(SR)_{16}$ and $Au_{24}(SR)_{20}$ has 4 valence electrons each, all of which disagree with the count in the superatom model. Recently, Cheng and Yang proposed the superatom-network (SAN) model to explain the electronic stability of non-spherical shells of metal clusters.[39] The electronic stability of the 4e thiolate-protected nanoparticles $Au_{18}(SR)_{14}$, $Au_{20}(SR)_{16}$ and $Au_{24}(SR)_{20}$ follows the SAN model and the Au_8^{4+} core of the three clusters should be viewed as two non-conjugate 4-center 2-electron (4c–2e) tetrahedral Au_4 superatoms.[39] The structure of $Au_{44}(SR)_{28}$ is theoretically predicted *via* DFT calculations and the $Au_{26}^{(+10)}$ core can be viewed as a network of eight tetrahedral Au_4 superatoms according to the SAN model.[40]

The super valence bond (SVB) model is another model proposed to explain the electronic stability of non-spherical shells of metal clusters.[41] The electronic shell of $Au_{38}(SR)_{24}$ has been studied, and the 23c–14e bi-icosahedral $Au_{23}^{(+9)}$ core is proved to be a superatomic molecule.[42] A very recent study is carried out on a pyramidal Au_{20} following the SVB model, and its superatomic 16c–16e core is bonded to four vertical Au atoms.[43] The $Au_{20}^{(+6)}$ core of the $[Au_{20}(PPhy_2)_{10}Cl_4]^{2+}$ nanocluster can be taken as a superatomic molecule bonded to two 11c–7e superatoms.[44] For the homoleptic $[Au(SR)]_n$ clusters with an Au/SR ratio of 1 : 1, there is no stacked Au core but exhibits only chain, ring, and catenane structures.[45]

As mentioned above, there have been a great number of studies on Au-L nanoclusters, which show a great diversity in geometric and electronic properties resulting from the unique energy landscape (EL) of Au-L systems.[24,29,46–53] However, still there has been no direct and overall study on the EL of Au-L systems. Using the Au_xCl_y binary system as a test case, we try to have a look at the EL of Au-L systems. Here we choose Cl representing L due to practical reasons. Moreover, we select the size $n = x + y = 20$, where the two magic number clusters $Au_{10}(SR)_{10}$ and Au_{20} are present.[20,45] In previous reports, the EL of binary nanoalloy clusters of the same cluster size is studied.[54] The low-lying isomers of the Au–Cl nanoclusters and the structural phase diagram (SPD) are obtained, showing great diversity and flexibility of electronic structures.

II. Computational details

The global minimum search for the isomers of the Au–Cl system is performed using a genetic algorithm (GA) coupled with DFT, which has been successfully applied in the structural prediction of a number of systems.[41,55–58] A GA is a search heuristic that mimics the process of natural selection.[59] This heuristic is routinely used to generate useful solutions to optimization and search problems. GAs belong to a larger class of evolutionary algorithms, which generate solutions to optimization problems using techniques inspired by natural evolution, such as inheritance, mutation, selection, and crossover.[60,61] DFT based GAs are very time-consuming, and for each cluster, more than 1000 samplings are optimized using DFT. The quantum chemical calculations are carried out on the GAUSSIAN 09 suite of programs.[62] In the optimization procedure, the Def2-TZVP basis set is used for Au which is obtained from the basis set exchange[63,64] that accounts for scalar relativistic effects, and the 6-311G* basis set is used for Cl using a generalized gradient approximation method using Tao–Perdew–Staroverov–Scuseria (GGA-TPSS)[65] without any symmetry constraint. The normal mode frequencies are also computed at the same level to ensure that they belong to real minima. The energies of the structures reported herein include the contribution of zero point energy (ZPE) corrections. For Au–Cl systems at $x \leq 9$, the multiplicities are set to 1, 3, 5, 7 and 9 to find the most stable isomers. The natural bond orbital (NBO)[66] analyses are calculated using the TPSS functional with a Lanl2dz basis set for Au and a 6-31G* basis set for Cl. To elucidate the nature of the chemical bonding, the adaptive natural density partitioning (AdNDP) is used to analyse the chemical bonding.[67] The AdNDP is based on the concept of the electron pair as the main element of chemical bonding models, which recovers both Lewis bonding elements (1c–2e and 2c–2e objects) and delocalized bonding elements (nc–2e). Molecular visualization is performed using MOLEKEL 5.4.[68]

III. Results and discussion

The lowest-lying equilibrium geometries and their symmetries of Au–Cl clusters are shown in Fig. 1, and the multiplicities of the Cl-rich clusters are also shown. It is worth noting that the structures of the Au–Cl clusters are broken up into pieces when $x \leq 4$, which are meaningless for the experiments in Au-L systems and are excluded in this work. We locate the global minimum structures and some relative stable isomers indexed in Roman numerals (such as I, II, III,... for Au_{20} according to energy from low to high) in Fig. S1 and S2, ESI.†

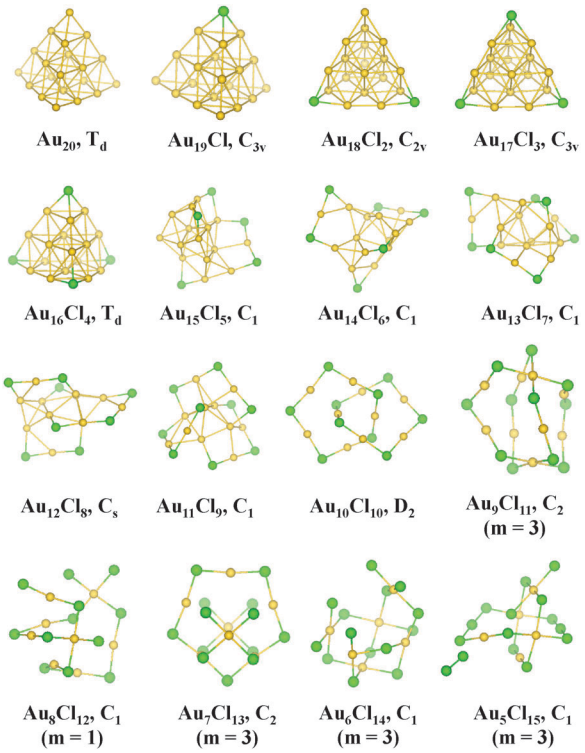

Fig. 1 Lowest-energy structures of Au_xCl_y ($x + y = 20$) clusters optimized at the TPSS/Def2-TZVP (Au) and 6-311G* (Cl) levels of theory. Au, yellow and Cl, green. At $x \leq 9$, enclosed are multiplicities of the molecules.

1. Structural phase diagram

To give a direct view of the structural evolution of the Au–Cl systems, Fig. 2 plots the structural phase diagram (SPD), a function of stability *versus* composition. The stability of the Au_xCl_y cluster is defined as the relative energy (E_{rel}) taking Au_{20} and Cl_2 as references. The calculated binding energy of Cl_2 at the computational level in this work (2.23 eV) is in good agreement with the experimental value (2.52 eV), indicating high reliability of the computational method.[69]

E_{rel} is calculated according to the formula:

$$E_{rel} = E(Au_xCl_y) - xE(Au_{20})/20 - yE(Cl_2)/2,$$

wherein $E(Au_xCl_y)$, $E(Au_{20})$ and $E(Cl_2)$ are the energies of Au_xCl_y, Au_{20} and Cl_2, respectively, including ZPE corrections. The magnitude of the absolute value of E_{rel} represents the relative stability of the cluster. The more negative E_{rel} is, the more stable is a cluster. As shown in the figure, it is obvious that E_{rel} decreases as x varies from 5 to 10, and increases as x changes from 10 to 20. At $x = 10$ with the stoichiometric ratio (1 : 1), E_{rel} is the most negative (−12.32 eV), indicating the highest stability. There is a sudden increase of E_{rel} when x changes from 10 to 9, where the clusters become Cl-rich. This indicates that it is difficult to obtain Cl-rich clusters in contrast to the 1 : 1 Au–Cl cluster. There is another sudden increase at $x = 5$, which is perhaps due to the instability of Au_5Cl_{15} that contains a separate Cl_2 molecule. Interestingly, the SPD curve at $x = 10$–20 is very smooth which indicates that the energy landscape of gold-rich Au–Cl clusters is very smooth and any ratio of Au and Cl is possible under certain experimental conditions.

2. Geometric and electronic structures

When $x = 10$, the stoichiometric ratio of Au and Cl is 1 : 1, and it presents a catenane structure. The canonical Cl–Au–Cl units emerge in the structure. $Au_{10}Cl_{10}$ is in D_2 symmetry, with interlocked pentamer rings. This catenane-like structure is a unique feature of homoleptic $[Au(I)–SR]_n$ ($n = 10$–12) complexes,[7,52] and low ratio Au–SR clusters, such as $Au_{24}(SR)_{20}$.[29,70,71]

When x is in the range of 11–20, the clusters are Au-rich, and the Au–Cl clusters can be viewed as Cl-protected gold nanoclusters. When x is in the scope of 9–5, the clusters are Cl-rich and the 5d electrons of Au atoms participate in bonding, resulting in high multiplicities.

2.1 $Au_{11}Cl_9$–$Au_{15}Cl_5$

$Au_{11}Cl_9$. $Au_{11}Cl_9$ is a 2e compound according to the superatom model.[32] The lowest-lying isomer (11I) contains one Au_5 rectangular pyramidal core protected by three –Cl–$(AuCl)_2$– staple motifs. Chemical bonding analysis by AdNDP reveals a 5c–2e bond with occupancy number (ON) = 1.84 |e| (Fig. 3a). Such an Au_5 2e-superatom has not been viewed in the experimentally produced Au–SR clusters. Moreover, there is one overprotected Au atom (labeled in purple and linked by two Cl atoms) in the Au_5 core, which is also not viewed in experiments.

Note that the tetrahedral Au_4 core has been theoretically predicted for small nanoparticles, such as in $Au_{10}(SR)_8$ and $Au_8(SR)_6$.[34,35] The corresponding Au–Cl isomer is 11IV (0.29 eV higher in energy than 11I), which also has an Au_4 core protected by one –Cl–$(AuCl)_3$– and one –Cl–$(AuCl)_4$– motifs. AdNDP analysis confirms the 4c–2e bond with ON = 1.77 |e| (Fig. 3b).

The trigonal bipyramidal Au_5 superatom is also viewed in 11V protected by three –Cl–$(AuCl)_2$– motifs, which is 0.37 eV higher in energy than 11I. AdNDP chemical bonding analysis confirms the 5c–2e bond with ON = 1.87 |e| (Fig. 3c).

$Au_{12}Cl_8$. $Au_{12}Cl_8$ is a 4e compound. The low-lying isomers follow the SAN ($2 \times 2e$) model in the electronic structure. Here we discuss the first four isomers 12I–IV with different SAN styles. Both 12I and 12II consist of a network of two non-conjugated tetrahedral Au_4 superatoms. AdNDP analysis reveals two 4c–2e bonds in 12I with ON = 1.76 |e| and 1.84 |e|, and both the ONs in 12II are 1.77 |e|. This binding pattern is in accordance with the experimentally synthesized 4e compounds $Au_{18}(SR)_{14}$, $Au_{20}(SR)_{16}$, $Au_{24}(SR)_{20}$ and $Au_{24}(SeR)_{20}$ clusters.[6,72–75]

12III also consists of a network of two non-conjugated Au_4 cores protected by four –Cl–Au–Cl– motifs. AdNDP analysis reveals two 4c–2e bonds with ON = 1.61|e|. However, there are two overprotected Au atoms (labeled in purple) and two naked Au atoms (marked in magenta) in the two Au_4 cores (Fig. 4c).

12IV has a unique vertex-sharing bitetrahedral Au_7 core which is composed of two conjugated Au_4 cores, ON = 1.83 |e| (Fig. 4d). Such a vertex-sharing Au_7 kernel is consistent with the experimentally determined structure of the $Au_{20}(SR)_{16}$ cluster.[73]

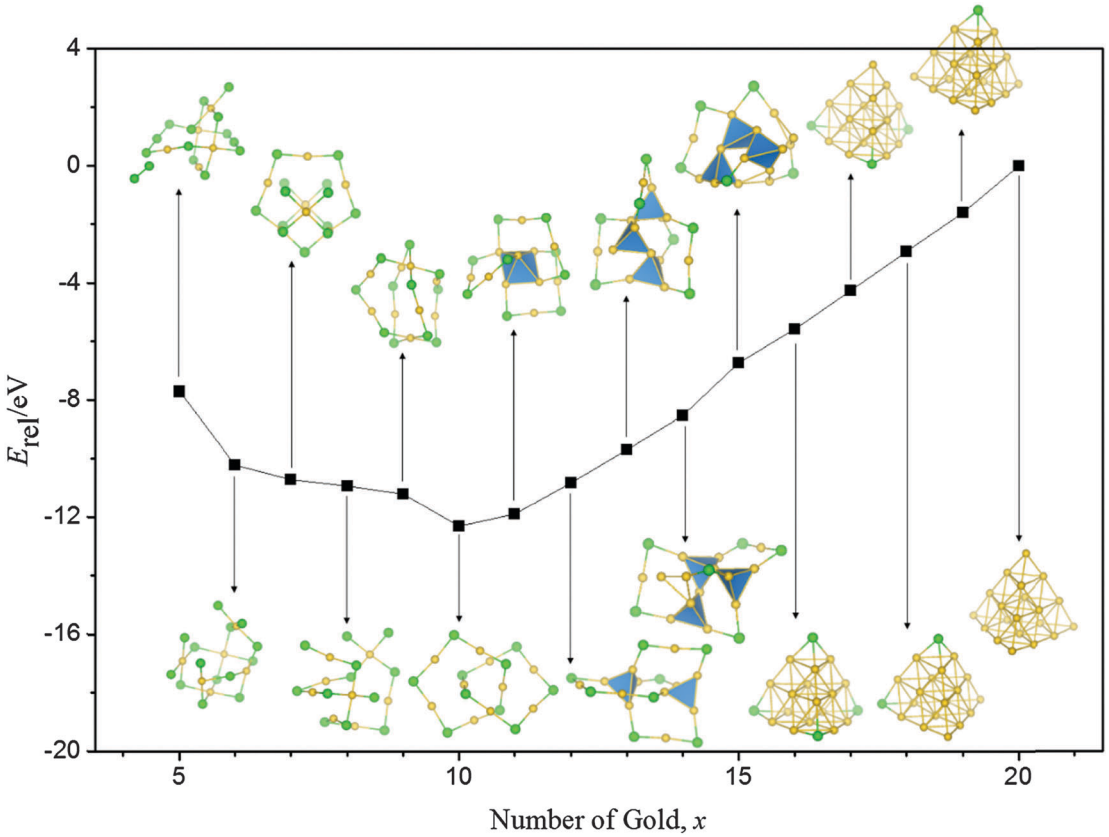

Fig. 2 Structural phase diagram (SPD) of Au_xCl_y ($x + y = 20$) clusters. E_{rel} is the energy of the molecule relative to Au_{20} and Cl_2 including zero point energies. The global minimum structures are also labeled, and the polyhedral models are used for $Au_{11}Cl_9$–$Au_{15}Cl_5$ clusters.

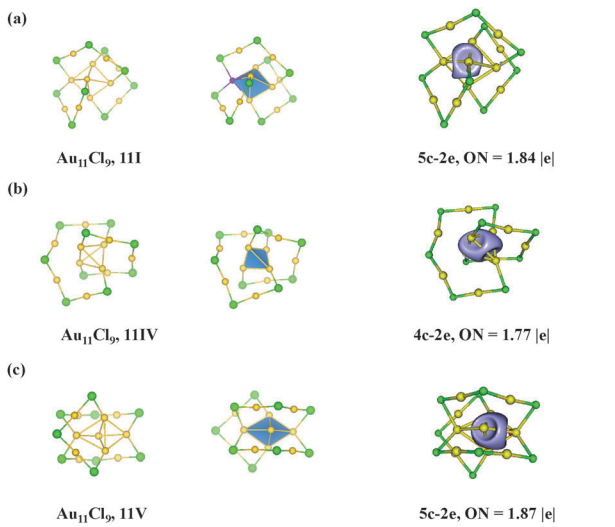

Fig. 3 Structures, superatom models and AdNDP localized natural bonding orbitals of the three isomers of $Au_{11}Cl_9$: (a) 11I, (b) 11IV and (c) 11V. Au, yellow and Cl, green.

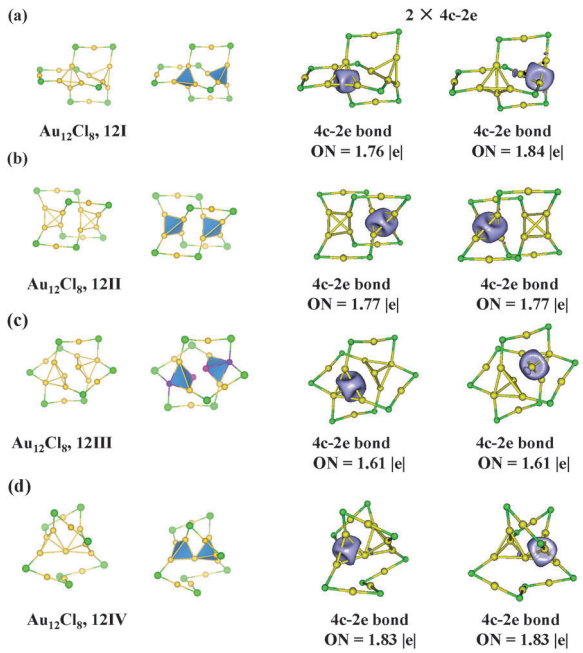

Fig. 4 Structures, superatom-network models and AdNDP localized natural bonding orbitals of the four isomers of $Au_{12}Cl_8$: (a) 12I, (b) 12II, (c) 12III and (d) 12IV. Au, yellow and Cl, green.

$Au_{13}Cl_7$. 13I is a 6e compound, and their cores can be viewed as a SAN ($3 \times 2e$) of three conjugated vertex-sharing tetrahedral Au_4 superatoms. Chemical bonding analysis by AdNDP reveals three conjugated 4c–2e bonds with ON = 1.77–1.82 |e| (Fig. 5a). There is one naked Au atom (marked with magenta) in one Au_4 superatom. The Au_4 vertex-sharing conformation has been revealed in the 12e $Au_{36}(SR)_{24}$ cluster.[76]

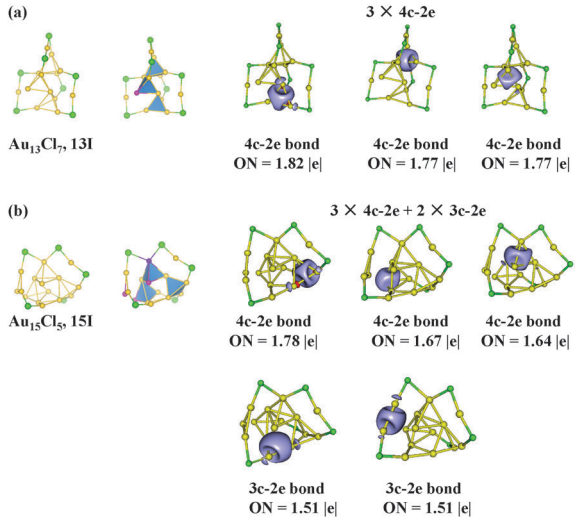

Fig. 5 Structures, superatom-network models and AdNDP localized natural bonding orbitals of (a) $Au_{13}Cl_7$ and (b) $Au_{15}Cl_5$. Au, yellow and Cl, green.

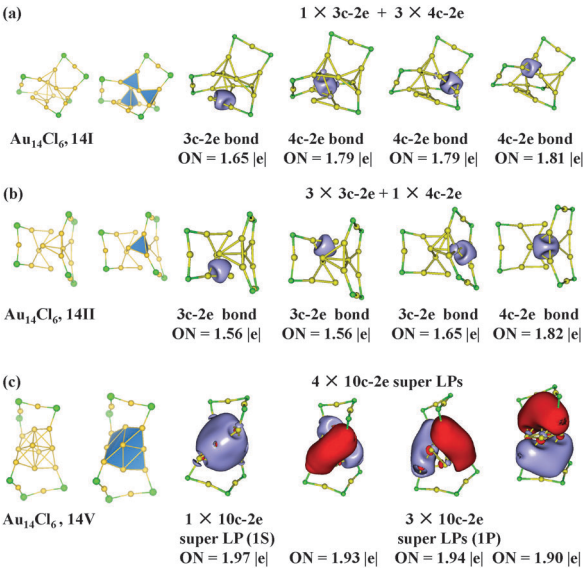

Fig. 6 Structures, superatom models and AdNDP localized natural bonding orbitals of the three isomers of $Au_{14}Cl_6$: (a) 14I, (b) 14II and (c) 14V. Au, yellow and Cl, green.

$Au_{14}Cl_6$. $Au_{14}Cl_6$ cluster is an 8e compound according to the superatom model. As shown in Fig. 6a, 14I can be viewed as a 4 × 2e SAN of one Au_3 superatom and three Au_4 superatoms stapled by two –Cl units and two –Cl–Au–Cl– units. In addition, the superatoms are vertex-sharing. The ON of the 3c–2e bond is 1.65 |e|, and those of the 4c–2e bonds are 1.79–1.81 |e|. Such a 3c–2e superatom is not viewed in experimentally produced Au–SR clusters. 14II is also a 4 × 2e SAN, which consists of three Au_3 superatoms and one Au_4 superatom stapled by three –Cl–Au–Cl– units and lies 0.49 eV higher in energy than 14I. The experimentally produced $Au_{28}(SR)_{20}$ cluster is a 4 × 2e SAN with four tetrahedral Au_4 2e-superatoms in the electronic structure.[77,78]

14V is an 8e-superatom, which consists of one tetrahedral Au_{10} core stapled by two –Cl–$(AuCl)_2$– units. AdNDP analysis reveals $1S^21P^6$ superatom orbitals in the tetrahedron (Fig. 6c). It is worth noting that 14V lies 0.97 eV higher in energy than 14I, indicating that the 4 × 2e SAN is favoured more than the 8e-superatom for Au–Cl systems.

$Au_{15}Cl_5$. 15I is a 10e compound, which can be viewed as a SAN of three Au_4 superatoms and two Au_3 superatoms stapled by three –Cl units and one –Cl–Au–Cl– unit (Fig. 5b). AdNDP reveals two 3c–2e bonds and three 4c–2e bonds. There are three naked Au atoms (marked with magenta) and one overprotected Au atom (labeled in purple) in 15I. The Au cores in 15I are not well protected by the staple motifs due to the lack of Cl, and it is not stable as shown in the SPD curve.

2.2 $Au_{16}Cl_4$–Au_{20}. It is well known that the global minimum structure of Au_{20} is a pyramid.[20,79,80] The calculated HOMO–LUMO gap is 1.91 eV, in agreement with the experimental value (1.77 eV).[20] According to our extensive global search, the global minimum structures of $Au_{16}Cl_4$, $Au_{17}Cl_3$, $Au_{18}Cl_2$ and $Au_{19}Cl$ are all based on the Au_{20} pyramid.

16I is a vertex-replaced Au_{20} pyramid, where the four Au atoms on the vertices are replaced by Cl. Similarly, 17I, 18I and 19I can be regarded as the three, two and one Au atoms on the vertices substituted by Cl, respectively.

The fully-filled 5d electrons in Au ($5d^{10}6s^1$) atoms of 16I, 17I, 18I, 19I and 20I clusters are mainly localized as LPs and $6s^1$ are free valence electrons. Recently, our group has investigated the chemical bonding in pyramidal Au_{20} using the SVB model.[43] Au_{20} can be viewed as a superatomic molecule, in which the superatomic 16c–16e core (T) is in D^3S hybridization bonded with four vertical Au atoms for a molecule-like (TAu_4) electronic shell-closure. Fig. 7 plots the AdNDP chemical bonding of 16I. As shown in the figure, there are six 16c–2e super LPs of T (super 1S, 1P and $1D_{x^2-y^2,z^2}$) and four 17c–2e T–Cl superσ-bonds in 16I. Thus, similar to Au_{20}, 16I can also be viewed as a superatomic molecule with four T–Cl superatom–atom bonds.

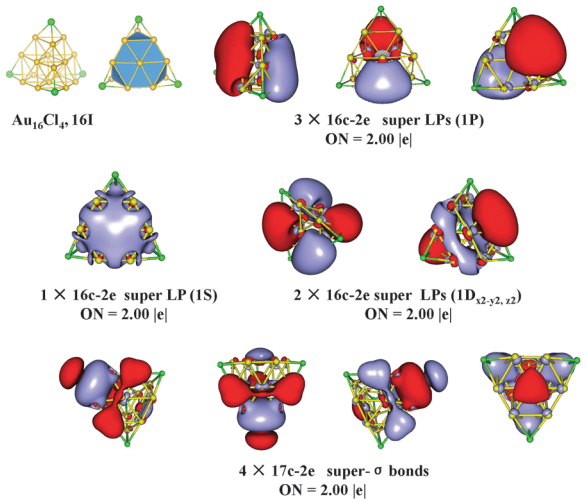

Fig. 7 Structure, superatomic molecular model and AdNDP localized natural bonding orbitals of $Au_{16}Cl_4$, 16I. Au, yellow and Cl, green.

Similarly, 17I, 18I and 19I are also superatomic molecules (see Fig. S3–S5, ESI†). Moreover, the linearity of the SPD curve at x = 16–20 indicates that the five global minimum structures are equally competitive based on the composition.

2.3 Au_9Cl_{11}–Au_5Cl_{15}. When x ranges from 9 to 5, the clusters are Cl-rich, and the 5d electrons of Au atoms participate in bonding, resulting in high multiplicities (Fig. 1).

Au_9Cl_{11}. 9I is in C_2 symmetry with a pentamer ring inserted into a hexamer ring, and the multiplicity is 3. The oxidation state of the two Au atoms on the two crossing points is +2.

Au_8Cl_{12}. 8I is a rather open structure in a singlet state with two crossing points. 8IV is a helix isomer (triplet state), in which the oxidation state of the four Au atoms on the four crossover points is +2.

Au_7Cl_{13}. 7I is a triplet C_2 structure, which has four intersection points. 7II, 7III and 7IV are in high multiplicities (3, 5 and 7), lying much higher in energy than 7I.

Au_6Cl_{14}. 6I is a triplet C_1 structure and has six crossover points. 6IV and 6V are in high multiplicities (7 and 5), each consisting of a quasi-cube unit and a Cl_2 molecule.

Au_5Cl_{15}. 5I is a triplet C_1 structure, which has two intersection points and one separate Cl_2 molecule.

3. Discussion

In this work, we replace −SR, −SeR, and $-PR_2$ with −Cl to investigate the energy landscape of the Au-L system. Jiang *et al.* performed a DFT study on $Au_{25}X_{18}^-$ (wherein X = F, Cl, Br and I) and found that the electronic structure of $Au_{25}Cl_{18}^-$ is almost identical to that of $Au_{25}(SR)_{18}^-$.[33] Moreover, there is high similarity between the frameworks of Au–S and Au–X systems. The structural patterns of Au–SR and Au–Cl systems are similar, indicating that the replacement of L by –Cl in Au-L systems is reasonable. This points to a way to predict the structures of Au–SR clusters by exploring Au–X clusters. Computationally, this greatly simplifies the process since the optimization of the Au–Cl system is much easier than that of the Au–SR system as the former contains less elements.

Pei *et al.* reviewed the structural evolution of Au–SR clusters.[81] The tetrahedral Au_4-units in $Au_{24}(SR)_{20}$ as well as the Au_6 and Au_8 cores in $Au_{12}(SR)_9^+$ and $Au_{18}(SR)_{14}$ support the existence of a major structural transition for Au–SR clusters with relatively small sizes. Moreover, the Au_{11}-core in $Au_{19}(SR)_{13}$ and the Au_{23}-core in $Au_{38}(SR)_{24}$ clusters can be viewed as a manifestation of the structural evolution of Au cores from small-to-medium sizes. It is worth noting that the cluster sizes in the review are relatively big with respect to our study system.

There are corresponding structures to most of the experimentally synthesized and theoretically predicted Au-L nanoclusters in our SPD. The $Au_{11}Cl_9$ cluster, which has an Au_4 core protected by staple motifs, corresponds to $Au_{10}(SR)_8$ and $Au_8(SR)_6$.[34,35] The $Au_{12}Cl_8$ cluster corresponds to the experimentally synthesized $Au_{18}(SR)_{14}$, $Au_{20}(SR)_{16}$, $Au_{24}(SR)_{20}$ and $Au_{24}(SeR)_{20}$ clusters.[6,72–75] $Au_{13}Cl_7$ follows the SAN (3 × 2e) model in the electronic structure, and their cores favour the vertex-sharing conformation revealed in the 12e compound $Au_{36}(SR)_{24}$.[76] $Au_{14}Cl_6$ follows a 4 × 2e SAN, which is associated with the experimentally synthesized $Au_{28}(SR)_{20}$ cluster in the electronic structure.[77,78] $Au_{15}Cl_5$ follows a 5 × 2e SAN. At x = 16–20, the global minimum structures of the Au–Cl system are all pyramidal structures. There are also differences between the electronic structures of Au–SR and Au–Cl systems. The Au_3 and Au_5 superatoms found in the Au–Cl system are not experimentally viewed in the Au–SR system. Of note, several structures of the Au–Cl system are not reasonable, for example, Au_5Cl_{15} and $Au_{15}Cl_5$, which are Cl-rich and Au-rich clusters, respectively. This may be due to the restriction of $x + y = 20$, which results in the lack of Au atoms and Cl atoms in Au_5Cl_{15} and $Au_{15}Cl_5$ clusters, respectively. There are naked Au atoms in gold cores of $Au_{15}Cl_5$ due to the lack of Cl atoms in the structure. Our investigation gives all the possible chemical bonding patterns for the studied Au–Cl system.

From our work, we can see that when we substitute –SR, –SeR, and $-PR_2$ ligands with –Cl in the Au-L system, the Au–Cl clusters still maintain the magic number series, and present gold cores and similar staple motifs. The great diversity of Au-L systems indicates that gold nanoparticles have their own universe in chemistry, and our work gives an overall perspective on this universe.

IV. Conclusions

In present work, the Au–Cl binary system is taken as a test case to investigate the EL of Au-L systems using the method combining GA with DFT. The sum of Au and Cl atoms is set to 20, in which the two magic number clusters $Au_{10}(SR)_{10}$ and Au_{20} are contained. We find a diverse set of global minimum structures and low-lying isomers for the system. The SAN and SVB models are used to characterize the bonding patterns. The Au–Cl binary system shows a great diversity and flexibility in electronic and geometric structures. This work gives a direct and overall view of the structural evolution of the Au–Cl system at relatively small size. The electronic structures of the Au–Cl clusters evolve from structures with high multiplicities to catenane conformation, structures containing superatoms, superatom networks and finally to superatomic molecules. There are corresponding structures to most of the experimentally synthesized and theoretically predicted Au-L nanoclusters in our SPD. This work indicates that the Au-L systems are of great diversity.

These insights are expected to offer some new perspectives in terms of structural evolution in Au-L nanoclusters. We believe that our work gives an overall and direct view of the universe of Au-L systems.

Acknowledgements

This work was supported by the National Natural Science Foundation of China (21273008). The calculations are carried out at the High-Performance Computing Centre of Anhui University.

References

1 J. Jung, S. Kang and Y. K. Han, *Nanoscale*, 2012, **4**, 4206–4210.
2 M. Z. Zhu, C. M. Aikens, M. P. Hendrich, R. Gupta, H. F. Qian, G. C. Schatz and R. C. Jin, *J. Am. Chem. Soc.*, 2009, **131**, 2490–2492.
3 H. T. Liu, X. G. Xiong, P. D. Dau, Y. L. Wang, J. Li and L. S. Wang, *Chem. Sci.*, 2011, **2**, 2101–2108.
4 P. Pyykkö, *Angew. Chem., Int. Ed.*, 2004, **43**, 4412–4456.
5 W. Lu, K. T. Chan, S. X. Wu, Y. Chen and C. M. Che, *Chem. Sci.*, 2012, **3**, 752–755.
6 Y. Negishi, K. Nobusada and T. Tsukuda, *J. Am. Chem. Soc.*, 2005, **127**, 5261–5270.
7 M. P. Johansson, A. Lechtken, D. Schooss, M. M. Kappes and F. Furche, *Phys. Rev. A: At., Mol., Opt. Phys.*, 2008, **77**, 053202.
8 A. Lechtken, C. Neiss, M. M. Kappes and D. Schooss, *Phys. Chem. Chem. Phys.*, 2009, **11**, 4344–4350.
9 W. Huang, S. Bulusu, R. Pal, X. C. Zeng and L. S. Wang, *ACS Nano*, 2009, **3**, 1225–1230.
10 L. Ferrighi, B. Hammer and G. K. Madsen, *J. Am. Chem. Soc.*, 2009, **131**, 10605–10609.
11 X. P. Xing, B. Yoon, U. Landman and J. H. Parks, *Phys. Rev. B: Condens. Matter Mater. Phys.*, 2006, **74**, 165423.
12 S. Bulusu and X. C. Zeng, *J. Chem. Phys.*, 2006, **125**, 154303.
13 M. Walter and H. Häkkinen, *Phys. Chem. Chem. Phys.*, 2006, **8**, 5407–5411.
14 S. Bulusu, X. Li, L. S. Wang and X. C. Zeng, *Proc. Natl. Acad. Sci. U. S. A.*, 2006, **103**, 8326–8330.
15 X. Gu, S. Bulusu, X. Li, X. C. Zeng, J. Li, X. G. Gong and L. S. Wang, *J. Phys. Chem. C*, 2007, **111**, 8228–8232.
16 M. Ji, X. Gu, X. Li, X. G. Gong, J. Li and L. S. Wang, *Angew. Chem., Int. Ed.*, 2005, **117**, 7281–7285.
17 A. Lechtken, D. Schooss, J. R. Stairs, M. N. Blom, F. Furche, N. Morgner, O. Kostko, B. von Issendorff and M. M. Kappes, *Angew. Chem., Int. Ed.*, 2007, **46**, 2944–2948.
18 B. Schaefer, R. Pal, N. S. Khetrapal, M. Amsler, A. Sadeghi, V. Blum, X. C. Zeng, S. Goedecker and L. S. Wang, *ACS Nano*, 2014, **8**, 7413–7422.
19 N. Shao, W. Huang, W. N. Mei, L. S. Wang, Q. Wu and X. C. Zeng, *J. Phys. Chem. C*, 2014, **118**, 6887–6892.
20 J. Li, X. Li, H. J. Zhai and L. S. Wang, *Science*, 2003, **299**, 864–867.
21 P. Gruene, D. M. Rayner, B. Redlich, A. F. van der Meer, J. T. Lyon, G. Meijer and A. Fielicke, *Science*, 2008, **321**, 674–676.
22 H. F. Zhang, M. Stender, R. Zhang, C. Wang, J. Li and L. S. Wang, *J. Phys. Chem. B*, 2004, **108**, 12259–12263.
23 P. D. Jadzinsky, G. Calero, C. J. Ackerson, D. A. Bushnell and R. D. Kornberg, *Science*, 2007, **318**, 430–433.
24 M. Z. Zhu, C. M. Aikens, F. J. Hollander, G. C. Schatz and R. C. Jin, *J. Am. Chem. Soc.*, 2008, **130**, 5883–5885.
25 H. F. Qian, Y. Zhu and R. C. Jin, *ACS Nano*, 2009, **3**, 3795–3803.
26 M. Z. Zhu, H. F. Qian and R. C. Jin, *J. Phys. Chem. Lett.*, 2010, **1**, 1003–1007.
27 X. K. Wan, Z. W. Lin and Q. M. Wang, *J. Am. Chem. Soc.*, 2012, **134**, 14750–14752.
28 T. D. Green, C. Y. Yi, C. J. Zeng, R. C. Jin, S. McGill and K. L. Knappenberger, *J. Phys. Chem. A*, 2014, **118**, 10611–10621.
29 D. E. Jiang, S. H. Overbury and S. Dai, *J. Am. Chem. Soc.*, 2013, **135**, 8786–8789.
30 M. Walter, M. Moseler, R. L. Whetten and H. Häkkinen, *Chem. Sci.*, 2011, **2**, 1583–1587.
31 P. R. Nimmala, S. Knoppe, V. R. Jupally, J. H. Delcamp, C. M. Aikens and A. Dass, *J. Phys. Chem. B*, 2014, **118**, 14157–14167.
32 M. Walter, J. Akola, O. Lopez-Acevedo, P. D. Jadzinsky, G. Calero, C. J. Ackerson, R. L. Whetten, H. Grönbeck and H. Häkkinen, *Proc. Natl. Acad. Sci. U. S. A.*, 2008, **105**, 9157–9162.
33 D. E. Jiang and M. Walter, *Nanoscale*, 2012, **4**, 4234–4239.
34 D. E. Jiang, W. Chen, R. L. Whetten and Z. F. Chen, *J. Phys. Chem. C*, 2009, **113**, 16983–16987.
35 D. E. Jiang, R. L. Whetten, W. D. Luo and S. Dai, *J. Phys. Chem. C*, 2009, **113**, 17291–17295.
36 D. E. Jiang, M. Walter and J. Akola, *J. Phys. Chem. C*, 2010, **114**, 15883–15889.
37 Y. Gao, N. Shao and X. C. Zeng, *ACS Nano*, 2008, **2**, 1497–1503.
38 Y. Gao, *J. Phys. Chem. C*, 2013, **117**, 8983–8988.
39 L. J. Cheng, Y. Yuan, X. Z. Zhang and J. L. Yang, *Angew. Chem., Int. Ed.*, 2013, **52**, 9035–9039.
40 Y. Pei, S. S. Lin, J. C. Su and C. Y. Liu, *J. Am. Chem. Soc.*, 2013, **135**, 19060–19063.
41 L. J. Cheng and J. L. Yang, *J. Chem. Phys.*, 2013, **138**, 141101.
42 L. J. Cheng, C. D. Ren, X. Z. Zhang and J. L. Yang, *Nanoscale*, 2013, **5**, 1475–1478.
43 L. J. Cheng, X. Z. Zhang, B. K. Jin and J. L. Yang, *Nanoscale*, 2014, **6**, 12440–12444.
44 Y. Yuan, L. J. Cheng and J. L. Yang, *J. Phys. Chem. C*, 2013, **117**, 13276–13282.
45 N. Shao, Y. Pei, Y. Gao and X. C. Zeng, *J. Phys. Chem. A*, 2009, **113**, 629–632.
46 A. Tlahuice and I. L. Garzón, *Phys. Chem. Chem. Phys.*, 2012, **14**, 3737–3740.
47 S. L. Christensen, M. A. MacDonald, A. Chatt, P. Zhang, H. F. Qian and R. C. Jin, *J. Phys. Chem. C*, 2012, **116**, 26932–26937.
48 A. Das, C. Liu, C. J. Zeng, G. Li, T. Li, N. L. Rosi and R. C. Jin, *J. Phys. Chem. A*, 2014, **118**, 8264–8269.
49 B. Assadollahzadeh and P. Schwerdtfeger, *J. Chem. Phys.*, 2009, **131**, 064306.
50 A. Dass, P. R. Nimmala, V. R. Jupally and N. Kothalawala, *Nanoscale*, 2013, **5**, 12082–12085.
51 W. Fa, C. F. Luo and J. M. Dong, *Phys. Rev. B: Condens. Matter Mater. Phys.*, 2005, **72**, 205428.
52 Y. Li, G. Galli and F. Gygi, *ACS Nano*, 2008, **2**, 1896–1902.
53 O. Lopez-Acevedo, J. Akola, R. L. Whetten, H. Gronbeck and H. Häkkinen, *J. Phys. Chem. C*, 2009, **113**, 5035–5038.
54 R. Ferrando, J. Jellinek and R. L. Johnston, *Chem. Rev.*, 2008, **108**, 845–910.
55 L. Ren, L. J. Cheng, Y. Feng and X. M. Wang, *J. Chem. Phys.*, 2012, **137**, 014309.

56 L. J. Cheng, *J. Chem. Phys.*, 2012, **136**, 104301.
57 L. F. Li and L. J. Cheng, *J. Chem. Phys.*, 2013, **138**, 094312.
58 Y. Yuan and L. Cheng, *J. Chem. Phys.*, 2012, **137**, 044308.
59 D. M. Deaven and K. M. Ho, *Phys. Rev. Lett.*, 1995, **75**, 288–291.
60 R. L. Johnston, *Dalton Trans.*, 2003, 4193–4207.
61 A. Shayeghi, D. Götz, J. Davis, R. Schaefer and R. L. Johnston, *Phys. Chem. Chem. Phys.*, 2015, **17**, 2104–2112.
62 M. J. Frisch, H. B. Schlegel, G. E. Scuseria, M. A. Robb, J. R. Cheeseman, G. Scalmani, V. Barone, B. Mennucci, G. A. Petersson, H. Nakatsuji, M. Caricato, X. Li, H. P. Hratchian, A. F. Izmaylov, J. Bloino, G. Zheng, J. L. Sonnenberg, M. Hada, M. Ehara, K. Toyota, R. Fukuda, J. Hasegawa, M. Ishida, T. Nakajima, Y. Honda, O. Kitao, H. Nakai, T. Vreven, J. A. Montgomery, J. E. Peralta, Jr., F. Ogliaro, M. Bearpark, J. J. Heyd, E. Brothers, K. N. Kudin, V. N. Staroverov, T. Keith, R. Kobayashi, J. Normand, K. Raghavachari, A. Rendell, J. C. Burant, S. S. Iyengar, J. Tomasi, M. Cossi, N. Rega, J. M. Millam, M. Klene, J. E. Knox, J. B. Cross, V. Bakken, C. Adamo, J. Jaramillo, R. Gomperts, R. E. Stratmann, O. Yazyev, A. J. Austin, R. Cammi, C. Pomelli, J. W. Ochterski, R. L. Martin, K. Morokuma, V. G. Zakrzewski, G. A. Voth, P. Salvador, J. J. Dannenberg, S. Dapprich, A. D. Daniels, O. Farkas, J. B. Foresman, J. V. Ortiz, J. Cioslowski and D. J. Fox, *Gaussian 09, Revision B.01*, Gaussian, Inc., Wallingford, CT, 2009.
63 K. L. Schuchardt, B. T. Didier, T. Elsethagen, L. S. Sun, V. Gurumoorthi, J. Chase, J. Li and T. L. Windus, *J. Chem. Inf. Model.*, 2007, **47**, 1045–1052.
64 F. Weigend and R. Ahlrichs, *Phys. Chem. Chem. Phys.*, 2005, **7**, 3297–3305.
65 J. Tao, J. P. Perdew, V. N. Staroverov and G. E. Scuseria, *Phys. Rev. Lett.*, 2003, **91**, 146401.
66 E. D. Glendening, J. K. Badenhoop, A. E. Reed, J. E. Carpenter, J. A. Bohmann, C. M. Morales and F. Weinhold, Theoretical Chemistry Institute, University of Wisconsin, Madison, WI, 2001.
67 D. Y. Zubarev and A. I. Boldyrev, *Phys. Chem. Chem. Phys.*, 2008, **10**, 5207–5217.
68 U. Varetto, *Swiss National Supercomputing Centre: Manno*, Switzerland, 2009.
69 K. P. Huber and G. Herzberg, *Constants of diatomic molecules*, Springer, 1979.
70 Y. Pei, R. Pal, C. Liu, Y. Gao, Z. Zhang and X. C. Zeng, *J. Am. Chem. Soc.*, 2012, **134**, 3015–3024.
71 S. S. Y. Chui, R. Chen and C. M. Che, *Angew. Chem.*, 2006, **118**, 1651–1654.
72 M. Z. Zhu, H. F. Qian and R. C. Jin, *J. Am. Chem. Soc.*, 2009, **131**, 7220–7221.
73 C. J. Zeng, C. Liu, Y. X. Chen, N. L. Rosi and R. C. Jin, *J. Am. Chem. Soc.*, 2014, **136**, 11922–11925.
74 Y. B. Song, S. X. Wang, J. Zhang, X. Kang, S. Chen, P. Li, H. T. Sheng and M. Z. Zhu, *J. Am. Chem. Soc.*, 2014, **136**, 2963–2965.
75 A. Das, T. Li, G. Li, K. Nobusada, C. J. Zeng, N. L. Rosi and R. C. Jin, *Nanoscale*, 2014, **6**, 6458–6462.
76 D. M. Chevrier, A. Chatt, P. Zhang, C. J. Zeng and R. C. Jin, *J. Phys. Chem. Lett.*, 2013, **4**, 3186–3191.
77 C. J. Zeng, T. Li, A. Das, N. L. Rosi and R. C. Jin, *J. Am. Chem. Soc.*, 2013, **135**, 10011–10013.
78 S. Knoppe, S. Malola, L. Lehtovaara, T. Bürgi and H. Häkkinen, *J. Phys. Chem. A*, 2013, **117**, 10526–10533.
79 J. L. Wang, G. H. Wang and J. J. Zhao, *Chem. Phys. Lett.*, 2003, **380**, 716–720.
80 R. B. King, Z. F. Chen and P. v. R. Schleyer, *Inorg. Chem.*, 2004, **43**, 4564–4566.
81 Y. Pei and X. C. Zeng, *Nanoscale*, 2012, **4**, 4054–4072.

